CHEMISTRY
A EUROPEAN JOURNAL

DOI: 10.1002/chem.200600376

Substitution of Hydrogen by Deuterium Changes the Regioselectivity of Ethylbenzene Hydroxylation by an Oxo–Iron–Porphyrin Catalyst

Sam P. de Visser*[a]

Abstract: Heme oxo–iron complexes are powerful oxygenation catalysts of environmentally benign hydroxylation processes. We have performed density functional theoretic calculations on a model system, that is, an oxo–iron–porphyrin (Por) complex [(Fe=O)Cl(Por)], and studied its reactivity toward a realistic substrate, namely, ethylbenzene. The calculations showed that the dominant reaction process in the gas phase is benzyl hydroxylation leading to 1-phenylethanol, with an energetic barrier of 9.1 kcal mol^{-1}, while the competing *para*-phenyl hydroxylation has a barrier 3.0 kcal mol^{-1} higher in energy. This benzyl hydroxylation barrier is the lowest C–H hydroxylation barrier we have obtained so far for oxo–iron–porphyrin complexes. Due to electronic differences between the intermediates in the phenyl and benzyl hydroxylation processes, the phenyl hydroxylation process is considerably stabilised over the benzyl hydroxylation mechanism in environments with a large dielectric constant. In addition, we calculated kinetic isotope effects of the substitution of one or more hydrogen atoms of ethylbenzene by deuterium atoms and studied its effect on the reaction barriers. Thus, in a medium with a large dielectric constant, a regioselectivity change occurs between [H_{10}]ethylbenzene and [D_{10}]ethylbenzene whereby the deuterated species gives phenol products whereas the hydrogenated species gives mainly 1-phenylethanol products. This remarkable metabolic switching was analysed and found to occur due to 1) differences in strength between a C–H versus a C–D bond and 2) stabilisation of cationic intermediates in a medium with a large dielectric constant. We have compared our calculations with experimental work on synthetic oxo–iron–porphyrin catalysts as well as with enzyme-reactivity studies.

Keywords: biomimetics · cytochrome P450 · density functional calculations · enzyme catalysis · isotope effects

Introduction

Cytochrome P450 enzymes are some of the strongest oxygenation catalysts in nature and are able to hydroxylate C–H bonds as well as epoxidise C=C double bonds.[1–7] As such, this class of enzymes is versatile and involved in many biochemical processes ranging from the detoxification of xenobiotics and the biosynthesis of hormones to the metabolism of drugs. The most commonly studied P450 enzyme is $P450_{cam}$, a bacteriological enzyme that hydroxylates camphor regiospecifically at the C5-position.[7–9] The active species of the enzyme (known as Compound I, Cpd I) remains elusive and as a result there are ongoing discussions regarding the oxidative power of Cpd I and the existence of possible alternative oxidants.[10,11] Cpd I contains a central oxo–iron group embedded in a heme and is bound to the peptide backbone via a thiolate linkage of a cysteinate side chain. It has been suggested that the precursor of Cpd I in the catalytic cycle, that is, the hydroperoxo–iron complex, may be a possible second oxidant.[12] Theoretical modelling of the catalytic properties of the oxo–iron versus the hydroperoxo–iron species, however, indicated that the hydroperoxo–iron species is a sluggish oxidant.[13] Recent studies by Nam et al.[14] on the oxo–iron versus the hydroperoxo–iron species of a nonheme complex confirmed that the hydroperoxo–iron complex is indeed a sluggish oxidant unable to compete with the oxo–iron species.

[a] Dr. S. P. de Visser
The Manchester Interdisciplinary Biocentre and
the School of Chemical Engineering and Analytical Science
The University of Manchester
131 Princess Street, Manchester M1 7DN (UK)
Fax: (+44) 161-306-4399
E-mail: sam.devisser@manchester.ac.uk

Supporting information (five tables with group spin densities; charges and relative energies of the various intermediates under different conditions; six figures with detailed geometry scans for various reaction processes) for this article is available on the WWW under http://www.chemeurj.org/ or from the author.

One of the most fascinating reaction processes of enzymes is metabolic switching, which leads to a regioselectivity change after some or all of the hydrogen atoms of the substrate have been replaced by deuterium atoms.[15,16] For instance, Atkins and Sligar[15] showed that 5,6-*exo*,*exo*-norcamphor-5,6-[D_2] was hydroxylated by $P450_{cam}$ at the C3-position, whereas the nondeuterated compound was hydroxylated at the C5-position. Studies on rat liver cytochrome P450 with toluene produced, in addition to benzyl hydroxylation, significant amounts of *o*-, *m*-, and *p*-cresol as side products.[17] A subsequent stepwise increase of the deuterium content in toluene led to an increase of the cresol products although the ratios between the different cresols stayed the same. Complete metabolic switching from benzyl hydroxylation to cresol formation occurred with [D_3]toluene, but further substitution of the ring hydrogen atoms by deuterium atoms had little effect.

Although a complete regioselectivity reversal with ethylbenzene as a substrate was not observed with rabbit liver microsomal $P450_{LM2}$, a significant change in the individual product distributions was obtained with deuterated substrates.[18,19] In particular, without deuterium substitution the reaction with ethylbenzene produced 1-phenylethanol in >99% yield, whereas with [D_2]ethylbenzene the obtained yields of 2-phenylethanol (1.1%) and *p*-ethylphenol (1.9%) were increased markedly. In addition, the absolute rate constants for these side reactions increased.[19] It was found that enzymatic activation of [D_1]ethylbenzene generally gives hydrogen abstraction rather than deuterium abstraction to form [D_1]-1-phenylethanol, that is, hydroxylation of [D_1]-(*R*)-phenylethane produced [D_1]-(*S*)-phenylethanol, and [D_1]-(*S*)-phenylethane gave [D_1]-(*R*)-phenylethane.[18,19] The hydroxylation of ethylbenzene by $P450_{LM2}$ gave a small preference for formation of the (*S*)-1-phenylethanol product, which implied that the reaction proceeded in a pro-*S* fashion possibly due to more favourable interactions of the pro-*S* form with the environment of the active site of the enzyme. The product ratios of the (*R*)- and (*S*)-1-phenylethanol were 48%:52% and only traces of 2-phenylethanol and ethylphenols were obtained.

Studies using a synthetic chiral binaphthyl iron–porphyrin catalyst for ethylbenzene hydroxylation resulted in stereoselective product formation, whereby [D_1]-(*R*)-phenylethane gave [D_1]-(*S*)-phenylethanol and [D_1]-(*S*)-phenylethane gave [D_1]-(*R*)-phenylethanol.[20] Moreover, the studies predicted a kinetic isotope effect (k_H/k_D) of 8.7 for [D_{10}]ethylbenzene when using this catalyst. Recent studies by Nam et al.[21] on the axial-ligand effect of oxo–iron–porphyrin catalysts on the hydroxylation of substrates showed remarkable regioselectivity differences between different catalysts. Thus, the *meso*-tetrakis(pentafluorophenyl)porphyrin (TPFPP)–oxo–iron catalyst with a chloride axial ligand [(Fe^{IV}=O)Cl-(TPFPP)$^{\bullet+}$] reacted with ethylbenzene to form 1-phenylethanol analogous to the P450 studies described above,[18,19] but the catalyst with a CH_3CN or CF_3SO_3 axial ligand reacted with ethylbenzene to form ethylbenzoquinone.[21] Moreover, replacement of ethylbenzene by its fully deuterated structure produced ethylbenzoquinone rather than 1-phenylethanol (Scheme 1), so that a complete regioselectivity reversal had occurred upon deuteration of the substrate.

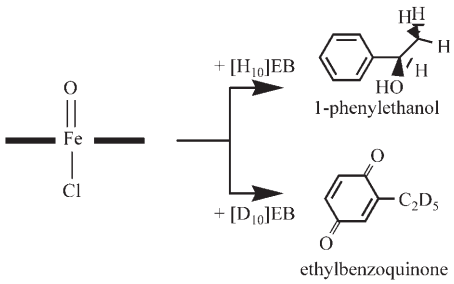

Scheme 1. The products obtained from the reaction of [(Fe^{IV}=O)Cl-(TPFPP)$^{\bullet+}$] with [H_{10}]ethylbenzene ([H_{10}]EB) and [D_{10}]ethylbenzene ([D_{10}]EB).[21]

Oxo–iron–porphyrin catalysts with chloride as the axial ligand have been used extensively, especially as epoxidising agents.[22] In particular, in order to compare the synthetic oxo–iron–porphyrin systems with biological systems in enzymes, such as P450, the effect of the axial ligand on the nature of the oxygenation process was studied and it was found that the oxygenation reactions are influenced by the axial ligand due to electron-withdrawing or electron-donating properties.[23]

To find the reasons behind this intriguing regioselectivity reversal upon deuteration of an ethylbenzene substrate, we decided to model this reaction by using density functional theory (DFT) methods. Thus, we studied competing hydroxylation mechanisms of ethylbenzene by an oxo–iron–porphyrin catalyst with chloride as the axial ligand [(Fe=O)Cl-(Por)] with reaction barriers leading to *p*-ethylphenol (product $\mathbf{P}_A$) and 1-phenylethanol (product $\mathbf{P}_B$), as shown in Scheme 2. Nam et al. showed that ring hydroxylation to

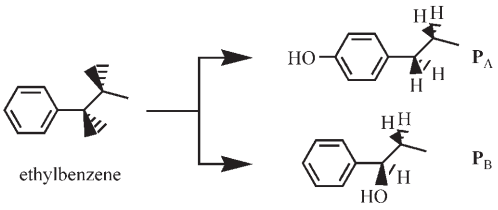

Scheme 2. Ethylbenzene hydroxylation leading to products $\mathbf{P}_A$ and $\mathbf{P}_B$ as studied in this work.

form phenol is the precursor of ethylbenzoquinone.[21] Currently, the reasons behind the regioselectivity change upon deuteration of a substrate remain unknown and no previous theoretical studies into this phenomena have been performed. Therefore, we deemed it timely to undertake a study into the effects that may influence the regioselectivity of hydroxylation by an oxo–iron–porphyrin catalyst. We per-

formed DFT calculations using a realistic substrate, that is, ethylbenzene, which is commonly used in experiments, and studied the reaction mechanisms leading to benzyl hydroxylation and phenol products. We describe the effects that influence the reaction barriers and make predictions of the reactivity patterns under various conditions.

Computational Methods

All calculations were performed by using commonly used procedures,[24,25] which will be briefly summarised here. Our model contained an oxo–iron–porphyrin catalyst with chloride as an axial ligand [(Fe=O)Cl(Por)] and the substrate used was ethylbenzene, so the total stoichiometry of the system was $C_{28}H_{22}ClFeN_4O$ and the overall charge was neutral. Because the [(Fe=O)Cl(Por)] system appears in close-lying quartet (high spin, HS) and doublet (low spin, LS) spin states, the oxidant will experience two-state reactivity patterns with reaction mechanisms on both spin surfaces.[26] The spin multiplicity in the structures is identified by the superscript 4 or 2 next to the label of the structure.

We used the unrestricted hybrid density functional method UB3LYP in combination with an LACVP basis set on iron, while the remaining atoms were described with a 6-31G basis set.[27,28] All structures described here are the result of a full optimisation (without constraints) in Jaguar 5.5[29] followed by an analytical frequency calculation in Gaussian 03.[30] All transition states were characterised with one imaginary frequency corresponding to the correct mode, whereas the local minima had real frequencies only. To test the effect of the basis set on the relative energies we performed single-point calculations in Jaguar using the triple-ζ quality basis set LACV3P+* on iron and the 6-311+G* basis set on the rest of the atoms.[28]

The effect of a dielectric constant on the relative energies was calculated by using the self-consistent reaction field (SCRF) procedure as implemented in Jaguar with a variety of dielectric constants (ε) mimicking chlorobenzene ($\varepsilon=5.7$, $r_P=2.72$ Å), 1,2-dichloroethane ($\varepsilon=10.65$, $r_P=2.51$ Å) and water ($\varepsilon=80.37$, $r_P=1.40$ Å), with r_P being the probe radius of the solvent.[29]

The kinetic isotope effect (KIE) for the replacement of one or more hydrogen atoms by deuterium atoms in the substrate was calculated by using the semiclassical Eyring (E) equation [Eq. (1)] using the free energies of activation ($\Delta G^{\ddagger}$) of the deuterium-substituted and reference systems as taken from the Gaussian frequency calculations.[31]

$$KIE_E = k_H/k_D = \exp\{(\Delta G^{\ddagger}{}_D - \Delta G^{\ddagger}{}_H)/RT\} \quad (1)$$

In this equation, R is the gas constant and T the temperature (298.15 K). The effect of tunnelling using the Wigner (W) correction on the KIE values was further calculated by multiplying KIE_E by the tunnelling ratio (Q_{tH}/Q_{tD}) as shown in Equations (2) and (3):

$$KIE_W = KIE_E \times \frac{Q_{tH}}{Q_{tD}} \quad (2)$$

$$Q_t = 1 + \frac{1}{24}\left(\frac{h\nu}{kT}\right)^2 \quad (3)$$

Here, k is the Boltzmann constant, h is the Planck constant and ν is the magnitude of the imaginary frequency in the transition state.

Results

Structure and electronic properties of [(Fe=O)Cl(Por)]: Let us start by briefly summarising the electronic and structural properties of the oxo–iron–porphyrin catalyst with chloride as the axial ligand, [(Fe=O)Cl(Por)], which analogously to the P450 systems we will label Compound I (Cpd I).[25] Figure 1 shows the singly occupied orbitals as well as the optimised geometries of ^{4,2}[(Fe=O)Cl(Por)]. The high-lying occupied and low-lying virtual orbitals of oxo–iron species are dominated by the 3d metal series that split into the typical t_{2g}–e_g splitting of which the three t_{2g} orbitals separate further into a nonbonding δ orbital in the plane of the porphyrin, which is doubly occupied, and two antibonding π* orbitals (π^*_{xz}, π^*_{yz}) for the Fe–O interaction.[32] The remaining two 3d-type orbitals are the virtual σ^*_{xy} orbital for the interactions of the metal with the pyrrole nitrogen atoms and the $\sigma^*_{z^2}$ for the antibonding Cl–Fe–O interaction. The metal d block is formally occupied with four electrons ($(\delta)^2(\pi^*_{xz})^1(\pi^*_{yz})^1$), hence the iron is in oxidation state IV. In addition, the system has a radical located on the porphyrin ring in a partially filled orbital that in D_{4h} symmetry has a_{2u} symmetry and for simplicity we use that notation here as well. This orbital mixes with an axial-ligand orbital (π_L) similarly to thiolate systems.[25,32] As the coupling between the singly occupied π* orbitals and the a_{2u} orbital is small, the electrons can be ferromagnetically coupled into a quartet spin state or antiferromagnetically coupled into an overall doublet spin state with occupation $(\delta)^2(\pi^*_{xz})^1(\pi^*_{yz})^1(a_{2u})^1$ (Figure 1).[32] The energy difference between the two spin states is very small (0.06 kcal mol^{-1} in favour of the HS state), so that Cpd I will experience a two-state reactivity pattern, whereby the quartet and doublet spin states give competing reaction mechanisms and reaction processes.[26,32] Thus, Cpd I with a chloride axial ligand has a similar pair of electronic ground states to the analogous heme oxo–iron systems such as P450 and horseradish peroxidase (HRP), in which the same electronic states were low lying.[32,33] Similarly to P450 and HRP, also with chloride as the axial ligand, the ordering of the

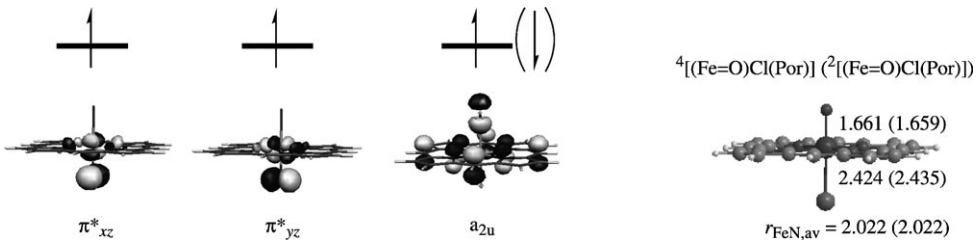

Figure 1. Singly occupied molecular orbitals (left) and optimised geometry of ^{4}[(Fe=O)Cl(Por)] (^{2}[(Fe=O)Cl(Por)]) with bond lengths in Å (right).

spin states varies under external perturbations such as a dielectric constant.[25]

Arene hydroxylation of ethylbenzene: The reaction mechanism for arene hydroxylation of ethylbenzene is shown in Scheme 3 and starts with an initial C–O bond-formation step whereby an intermediate (^{4,2}**A**) is created. This intermediate is a radical in the quartet spin state but a cation in the doublet spin state (vide infra). Subsequently, a proton transfer from the *ipso* position to one of the nitrogen atoms of the porphyrin ring takes place to create the proton-transfer complexes (^{4,2}**PT**). From this point onward, the two spin-state surfaces converge again and produce the same structures and intermediates, and the proton is reshuttled either to the oxygen atom to produce *p*-ethylphenol (^{4,2}**P**$_A$) or to the C3 carbon atom to form 4-ethylcyclohexa-2,4-dienone (^{4,2}**P**$_C$). The mechanism as described here shows some similarities with calculations on a smaller model system using benzene as a substrate, but, as will be discussed below, there are some critical differences. A direct hydrogen transfer within the aromatic group was ruled out because previous studies showed this process to be too energetically demanding.[34]

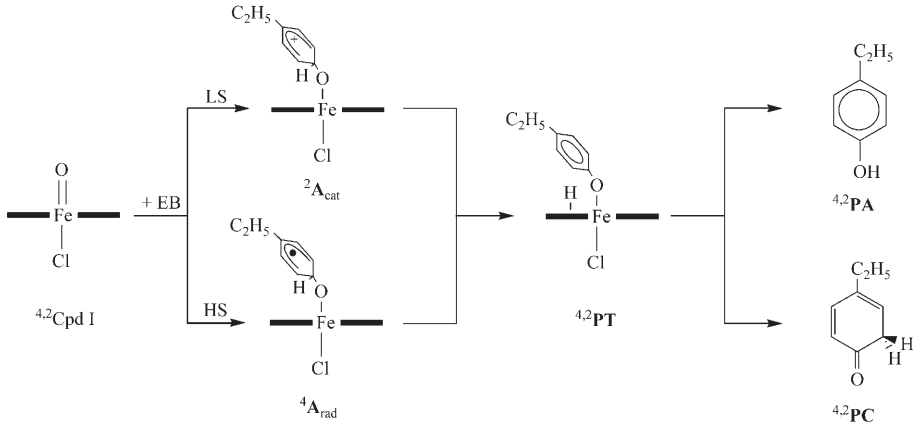

Scheme 3. Reaction mechanism for arene hydroxylation as studied in this work. EB stands for ethylbenzene, LS is the low spin and HS is the high spin.

Figure 2 shows the potential-energy profile for arene hydroxylation of ethylbenzene at the *para* position leading to *p*-ethylphenol (^{4,2}**P**$_A$) and 4-ethylcyclohexa-2,4-dienone (^{4,2}**P**$_C$), and the optimised geometries are depicted in Figure 3. As can be seen from Figure 2, the rate-determining step on both surfaces is the initial C–O bond-formation step via ^{4,2}**TS**$_A$ with barriers of 16.9 (HS) and 12.1 kcal mol^{-1} (LS). This unusual large separation between the HS and LS surfaces is the result of the formation of a radical intermediate ^{4}**A**$_{rad}$ on the high-spin surface, while a cationic intermediate ^{2}**A**$_{cat}$ is created on the low-spin surface. Thus, simultaneous to the C–O bond formation is an electron transfer from the substrate into the a_{2u} orbital, thereby creating an intermediate (^{4}**A**$_{rad}$) with orbital occupation $(\delta)^2(\pi^*_{xz})^1(\pi^*_{yz})^1(a_{2u})^2(\varphi_{Ph})^1$ (φ_{Ph} being the radical orbital on the benzene ring), and the iron retains the IV oxidation state. On the other hand, in ^{2}**A**$_{cat}$ an electronic situation is created whereby the iron is in oxidation state III with a cationic substrate due to a molecular orbital occupation of $(\delta)^2(\pi^*_{xz})^2(\pi^*_{yz})^1(a_{2u})^2(\varphi_{Ph})^0$. When using benzene as a substrate, a close-lying radical state (^{2}**A**$_{rad}$) was also found in the LS state with orbital occupation $(\delta)^2(\pi^*_{xz})^1(\pi^*_{yz})^1(a_{2u})^2(\varphi_{Ph})^1$.[34] Attempts to optimise ^{2}**A**$_{rad}$ here failed because the wave function converged to the more stable cationic configuration (^{2}**A**$_{cat}$). Therefore, we conclude that with ethylbenzene as a substrate the cationic

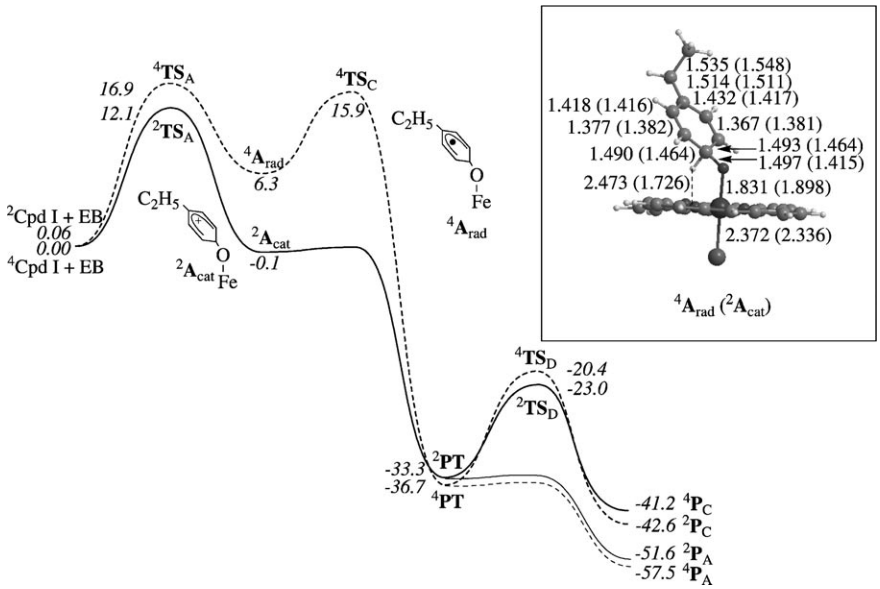

Figure 2. Potential-energy profile for the arene activation of ethylbenzene (EB) by ^{4,2}Cpd I. All energies are in kcal mol^{-1} relative to the isolated reactants and have been taken from LACV3P+* values with ZPE corrections at the LACVP level of theory. The inset show the optimised geometries of ^{4}**A**$_{rad}$ (^{2}**A**$_{cat}$) with bond lengths in Å.

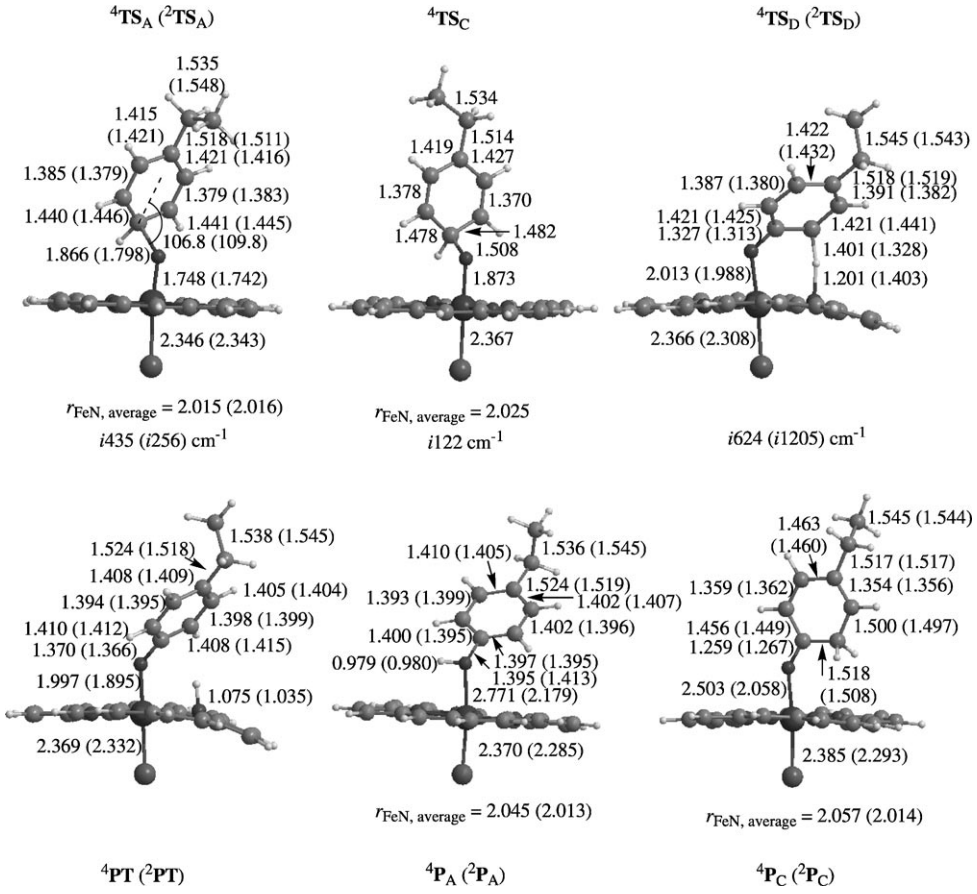

Figure 3. Optimised geometries of critical points along the phenyl hydroxylation pathway. Bond lengths are in Å, angles in degrees and imaginary frequencies of the transition-state structures in cm^{-1}.

states are much lower lying than those with benzene as a substrate and as a result the energy difference between $^2\mathbf{A}_{cat}$ and $^2\mathbf{A}_{rad}$ is much larger. Thus, whereas with benzene as a substrate the processes leading to $^2\mathbf{A}_{cat}$ and $^2\mathbf{A}_{rad}$ were found to be competitive, when using ethylbenzene as a substrate there is a clear preference of a pathway via $^2\mathbf{A}_{cat}$ over $^2\mathbf{A}_{rad}$. The energy difference between $^4\mathbf{TS}_A$ and $^2\mathbf{TS}_A$ is 4.8 kcal mol^{-1}, while $^4\mathbf{A}_{rad}$ and $^2\mathbf{A}_{cat}$ are 6.4 kcal mol^{-1} apart. By contrast, these energy differences are only 2.5 and 1.7 kcal mol^{-1}, respectively, for the reaction of benzene with [(Fe=O)(Por)(SH)],[34] which supports our conclusion that with ethylbenzene as a substrate the cationic states are considerably stabilised.

The conversion of the intermediate $^2\mathbf{A}_{cat}$ into $^2\mathbf{PT}$ is almost barrierless due to identical orbital occupation in the structures. However, the conversion of $^4\mathbf{A}_{rad}$ into $^4\mathbf{PT}$ requires the transfer of an electron from the substrate into the metal 3d system, that is, into the σ_{z^2}* orbital, and hence a significant barrier ($^4\mathbf{TS}_C$) is encountered. Therefore, the cationic intermediate $^2\mathbf{A}_{cat}$ will have a very short lifetime and almost instantaneously donate the proton to the porphyrin ring to form $^2\mathbf{PT}$, while on the HS surface the lifetime of the radical will be longer.

The reaction mechanism bifurcates in $^{4,2}\mathbf{PT}$, because the proton located on the nitrogen atom of the porphyrin ring can be reshuttled to the oxygen atom to form *p*-ethylphenol ($^{4,2}\mathbf{P}_A$) via an almost barrierless process or to the C3 carbon atom to produce 4-ethylcyclohexa-2,4-dienone ($^{4,2}\mathbf{P}_C$). The latter process encounters a significant barrier ($^{4,2}\mathbf{TS}_D$), but this is well below the energy of $^{4,2}\mathbf{A}$, therefore, it is entirely possible that part of its energy is retained and can be used to cross the barrier and produce $^{4,2}\mathbf{P}_C$ side products.

Alkyl hydroxylation of ethylbenzene: Figure 4 shows optimised geometries for the hydroxylation of the benzyl carbon atom of ethylbenzene by ^{4,2}Cpd I, and the potential-energy surface is depicted in Figure 5. In agreement with previous hydroxylation studies of oxo–iron–porphyrin systems, the initial reaction is a hy-

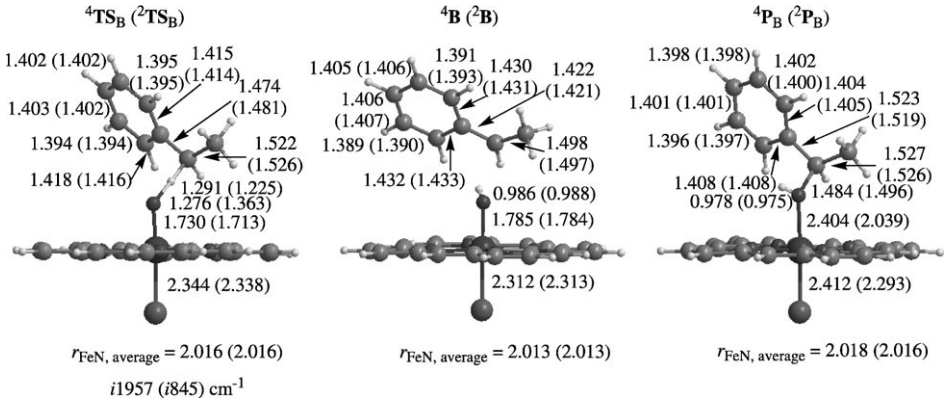

Figure 4. Optimised geometries of critical points along the benzyl hydroxylation pathway of ethylbenzene by ^{4,2}Cpd I. All structures were fully optimised with Jaguar 5.5 using UB3LYP/LACVP. Bond lengths are in Å and the imaginary mode of the transition states is in cm^{-1}.

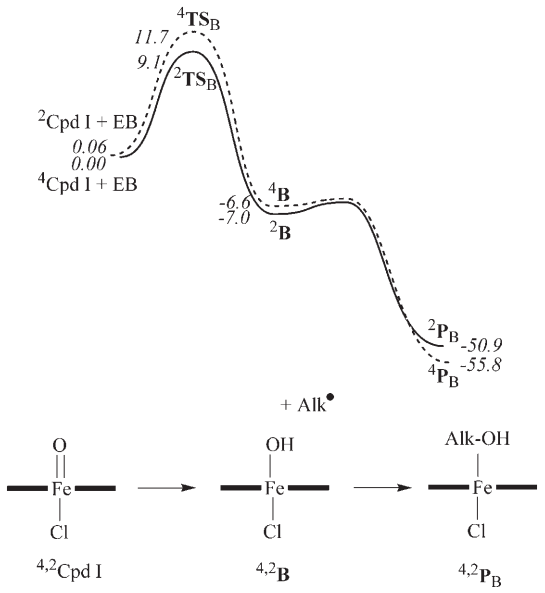

Figure 5. Energy landscape for the benzyl hydroxylation of ethylbenzene (EB) by ^{4,2}Cpd I. All energies were obtained at the LACV3P+* level of theory with ZPE at the LACVP level of theory and are in kcal mol^{-1} relative to the isolated reactants. Alk is the group left over from ethylbenzene after hydrogen abstraction.

drogen abstraction via ^{4,2}**TS**$_B$ leading to a hydroxo–iron species with a nearby substrate radical (intermediate ^{4,2}**B**).[31,35,36] In a subsequent step, the radical rebounds to the hydroxo group and the alcohol product is formed (^{4,2}**P**$_B$). On both spin surfaces, the rebound barrier is negligible, which implies that the radical intermediates will have very short lifetimes. Nevertheless, the rate-determining step is the initial hydrogen abstraction via ^{4,2}**TS**$_B$ with a barrier of 9.1 kcal mol^{-1} on the LS surface and 11.7 kcal mol^{-1} on the HS surface. The LS barrier is the lowest C–H hydroxylation barrier we have thus far calculated for oxo–iron–porphyrin models.[32,36] Geometrically, the two transition states are very much alike, with the only difference being the location of the transferring hydrogen atom. In ^{4}**TS**$_B$, the hydrogen atom is almost midway between the donor carbon atom and the acceptor oxygen atom (r_{CH} = 1.291 Å, r_{OH} = 1.276 Å), whereas in ^{2}**TS**$_B$ the transition state is somewhat earlier on the reaction coordinate (r_{CH} = 1.225 Å, r_{OH} = 1.363 Å).

Energetically, the barriers are much lower than those obtained for the arene activation pathway of Figure 2, therefore, the benzyl hydroxylation via ^{2}**TS**$_B$ will be the dominant pathway in the gas phase, in agreement with experimental observations of P450 enzyme reactions as well as with synthetic catalysts.[18–21] In the next sections we will show how the relative energies of the four rate-determining transition states ^{4,2}**TS**$_A$ and ^{4,2}**TS**$_B$ vary under the influence of a dielectric constant and hydrogen–deuterium substitution.

Effect of the dielectric constant on the relative energies of ^{4,2}TS$_A$ and ^{4,2}TS$_B$: The rate-determining barrier in both the arene hydroxylation and phenyl hydroxylation mechanisms is the initial reaction barrier, that is, **TS**$_A$ and **TS**$_B$. Therefore, we tested the effect of the environment on the relative energies of ^{4,2}**TS**$_A$ and ^{4,2}**TS**$_B$ by the addition of a dielectric constant to the calculations using the SCRF model as implemented in Jaguar 5.5. Previously, we showed that a dielectric constant and hydrogen-bonding interactions can change the regioselectivity of propene oxidation by a P450 model Cpd I from dominant epoxidation in the gas phase to C–H hydroxylation in an enzyme-mimicked environment.[31a,37] Moreover, electrostatic interactions have been shown to determine the electronic ground-state properties of cytochrome *c* peroxidase and ascorbate peroxidase.[24a] Table 1 shows the relative energies of ^{4,2}**TS**$_A$ and ^{4,2}**TS**$_B$ under various conditions. In all cases ^{2}**TS**$_B$ is the lowest-lying reaction barrier, which implies that benzyl hydroxylation will be the most abundant process. However, in systems with a large dielectric constant ^{2}**TS**$_A$ is considerably stabilised and comes to within 1.3 kcal mol^{-1} of ^{2}**TS**$_B$. This is not surprising because ^{2}**TS**$_A$ corresponds to a transition state leading to a cationic intermediate, which should be considerably stabilised in a polar solvent. By contrast, ^{4}**TS**$_A$ leads to a radical intermediate and is destabilised in systems with a large dielectric constant. In conclusion, the calculations with a dielectric constant added indicate that the ^{2}**TS**$_A$ and ^{2}**TS**$_B$ processes are competitive in polar solvents, and presumably other small external perturbations can change the regioselectivity.

Table 1. Relative energies [kcal mol^{-1}] of ^{4,2}**TS**$_A$ and ^{4,2}**TS**$_B$ under the influence of a dielectric constant (ε).[a]

	ε = 1	ε = 5.7	ε = 10.65	ε = 80.37
^{4}**TS**$_A$	7.9	7.9	8.2	8.6
^{2}**TS**$_A$	3.1	2.5	2.5	1.3
^{4}**TS**$_B$	2.6	2.6	2.8	2.3
^{2}**TS**$_B$	0.0	0.0	0.0	0.0

[a] The gas-phase (ε = 1) energy was calculated with LACV3P+* with ZPE and dielectric medium corrections were calculated at the LACVP level of theory.

The group spin densities of ^{2}**TS**$_A$ and ^{2}**TS**$_B$ obtained at three different dielectric constants, namely the gas phase (ε = 1), ε = 10.65 and ε = 80.37, are shown in Figure 6. As can be seen from Figure 6, the hydrogen-abstraction transition state (^{2}**TS**$_B$) shows little spin-density change, and consequently limited charge redistribution, with the addition of a dielectric constant. By contrast, the arene-activation transition state (^{2}**TS**$_A$) shows much greater spin density and charge changes with the addition of a dielectric constant. Because ^{2}**TS**$_A$ leads to a cationic intermediate (^{2}**A**$_{cat}$, see Figure 2 above), a positive charge is building up on the arene ring ($Q_{C_6H_5}$ = 0.43 in the gas phase), which increases to 0.54 with ε = 80.37. As a result, ^{2}**TS**$_A$ is stabilised with respect to ^{2}**TS**$_B$ as indeed observed from the relative energies in Table 1.

Hydrogen–deuterium substitution: Kinetic isotope effects for substitution of one or more hydrogen atoms by deuterium atoms in ethylbenzene were calculated for ^{4,2}**TS**$_A$ and

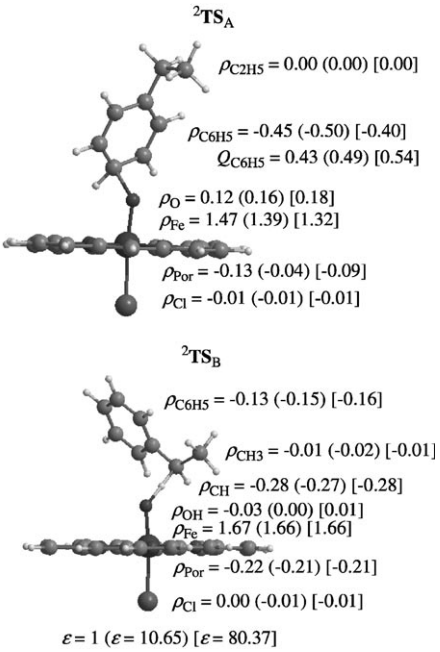

Figure 6. Group spin densities (ρ) and charges (Q) of ^{2}**TS**$_A$ and ^{2}**TS**$_B$ as calculated in the gas phase and in dielectric constants of $\varepsilon = 10.65$ (in parentheses) and of $\varepsilon = 80.37$ (in square brackets).

^{4,2}**TS**$_B$ with the Eyring and Wigner models, as described in the Computational Methods section, and are shown in Table 2. The hydrogen atoms of ethylbenzene are arranged in five groups as identified in Scheme 4 with the labels a–e.

Table 2. Kinetic isotope effects as calculated with the Eyring equation (KIE_E) and Wigner correction (KIE_W) and free energies of activation ($\Delta G^{\neq}$ in kcal mol^{-1}) of [H_{10}]ethylbenzene, [D_2]ethylbenzene and [D_{10}]ethylbenzene.[a]

	^{4}**TS**$_A$		^{2}**TS**$_A$		^{4}**TS**$_B$		^{2}**TS**$_B$	
	KIE_E	KIE_W	KIE_E	KIE_W	KIE_E	KIE_W	KIE_E	KIE_W
D_1^c	1.2	1.2	1.1	1.1	7.4	11.1	5.5	6.2
D_1^d	1.1	1.1	1.0	1.0	1.1	1.1	1.1	1.1
D_2^{cd}	1.3	1.3	1.1	1.1	7.9	12.0	5.8	6.6
D_3^e	1.1	1.1	1.0	1.0	1.1	1.1	1.1	1.1
D_1^a	0.9	0.9	0.9	0.9	1.0	1.0	1.0	1.0
D_5^{ab}	0.9	0.9	0.9	0.9	1.0	1.0	1.0	1.0
D_{10}^{abcde}	1.1	1.1	0.9	0.9	8.0	12.1	5.9	6.7
$\Delta G^{\neq}(H_{10})$[b]	30.8		25.6		23.8		23.4	
$\Delta G^{\neq}(D_2)$[c,d]	30.9		25.6		25.1		24.5	
$\Delta G^{\neq}(D_{10})$[c]	30.8		25.5		25.1		24.5	

[a] Isotopic substitution of the hydrogen atoms of ethylbenzene is defined as in Scheme 4: H^a-$C_6H_4^b$-CH^cH^d-CH_3^e in which H^c is the hydrogen atom transferred to the oxo–iron group. The superscript identifies the hydrogen atoms being replaced by deuterium atoms and the subscript is the total number of isotopic substitutions. For example, in D_3^e all three hydrogen atoms of the methyl group were replaced by deuterium atoms and D_{10}^{abcde} is fully deuterated ethylbenzene. [b] Free energy of activation as calculated by using energies at LACV3P+* with ZPE; thermal corrections and entropies were calculated at the LACVP level of theory. [c] Free energy of activation of deuterated ethylbenzene using energies at LACV3P+* with ZPE; thermal corrections and entropies were calculated at the LACVP level of theory. [d] Isotopic substitution of both benzyl hydrogen atoms, that is, D_2^{cd}.

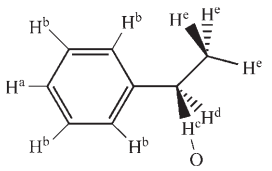

Scheme 4. Labelling of the hydrogen atoms in ethylbenzene.

Thus, the hydrogen atom transferred in the benzyl hydroxylation process is labelled H^c, whereas the other benzyl hydrogen atom is labelled H^d. Generally, isotopic substitution of hydrogen atoms attached to the phenyl group (atoms H^a and H^b) or as part of the terminal methyl group (atoms H^e) have little effect on the KIE values. Even the secondary KIE for the replacement of hydrogen atom H^d by a deuterium atom is very small.

Because the barriers ^{4,2}**TS**$_A$ are essentially C–O bond-formation barriers, the effect of isotopic substitution is only marginal and is typically $k_H/k_D < 1.2$. Note that an inverse KIE value was obtained for ^{4,2}**TS**$_A$ when one or more of the phenyl hydrogen atoms (H^a, H^b) were substituted by deuterium atoms ($k_H/k_D = 0.9$). As the KIE values of the C–O bond-formation barriers (^{4,2}**TS**$_A$) are close to unity, the free energy of activation values for [H_{10}]ethylbenzene and [D_{10}]ethylbenzene are almost identical: 25.6 versus 25.5 kcal mol^{-1}, respectively, for ^{2}**TS**$_A$. By contrast, the hydrogen-abstraction barriers ^{4,2}**TS**$_B$ have a large kinetic isotope effect ranging from $k_H/k_D = 6.7$ for ^{2}**TS**$_B$ to 12.1 for ^{4}**TS**$_B$ for the fully deuterated substrate. These values are typical for oxo–iron–porphyrin systems and agree well with calculations on heme catalysts, such as P450 systems.[31] By using a chiral binaphthyl iron–porphyrin catalyst, Groves and Viski[20] obtained $k_H/k_D = 8.7$ for ethylbenzene hydroxylation, which is midway between our HS and LS values. Moreover, their studies revealed that [D_1]-1-phenylethane was converted into [D_1]-1-phenylethanol so that the reaction proceeded by hydrogen abstraction and not by deuterium abstraction.[20] This is in agreement with our observations (Table 2) that the barrier for hydrogen abstraction is lower in energy than the barrier for deuterium abstraction. Our calculated KIE values here agree very well with those obtained for propene hydroxylation by [(Fe=O)Cl(Por)] and [(Fe=O)(Por)(SH)] catalysts, for which the KIE value for the HS surface was usually higher than that for the LS surface.[25,31a] This difference can be attributed to the much larger imaginary frequency for ^{4}**TS**$_B$ (i1957.3 cm^{-1}) relative to ^{2}**TS**$_B$ (i845.2 cm^{-1}). As a consequence of this large isotope effect of ^{4,2}**TS**$_B$, the free energy of activation ($\Delta G^{\neq}$) of the fully deuterated substrates increases from 23.8 to 25.1 kcal mol^{-1} (HS) and from 23.4 to 24.5 kcal mol^{-1} (LS). Therefore, because deuteration of ethylbenzene destabilises the hydrogen-abstraction barriers (^{4,2}**TS**$_B$), but does not change the free energy of the C–O bond-formation barrier (^{2}**TS**$_A$), as a result, the three transition states become competitive and within 1 kcal mol^{-1} of each other. Indeed, as observed by White et al.,[19] the amount of phenol side products in the reaction of ethylbenzene with $P450_{LM2}$ increased significantly upon deuteration of the substrate.

Discussion

In this work we present DFT studies for the reaction of ^{4,2}[(Fe=O)Cl(Por)] with ethylbenzene, and the potential-energy landscape for the processes leading to 1-phenylethanol ($\mathbf{P_B}$), *p*-ethylphenol ($\mathbf{P_A}$) and 4-ethylcyclohexa-2,4-dienone ($\mathbf{P_C}$) are summarised in Figure 7. The reactions proceed through two-state reactivity on competing quartet and doublet spin-state surfaces. The dominant pathway in the gas phase is the mechanism via $^2\mathbf{TS_B}$ leading to 1-phenylethanol with a barrier of 9.1 kcal mol^{-1}. This barrier is much lower than those obtained for a series of typical hydrogen-abstraction reactions by P450 model systems,[36] and is also much lower than the epoxidation of propene by the same catalyst (11.7 kcal mol^{-1}).[25] Therefore, [(Fe=O)Cl(Por)] is a very efficient catalyst especially for the hydroxylation of C–H bonds and is more efficient than thiolate-ligated models. The reaction mechanisms obtained here for the hydrogen-abstraction and phenyl-hydroxylation processes are similar to those obtained before for thiolate-ligated models using smaller substrates.[31,34] The competing processes leading to phenol or cyclohexadienone products (via $^{4,2}\mathbf{TS_B}$) start with C–O bond formation, followed by shuttling of the *ipso* proton to the porphyrin ring and reshuttling of this proton to the oxo group to form the products. The phenyl hydroxylation barrier $^2\mathbf{TS_A}$ is only 12.1 kcal mol^{-1}, whereas for benzene hydroxylation by [(Fe=O)(Por)(SH)] a barrier of 18.1 kcal mol^{-1} was obtained.[34] When using ethylbenzene as a substrate, the cationic intermediates are significantly more stable than the radical intermediates in the phenyl hydroxylation mechanism, which also results in a significant lowering of the absolute value of the $^2\mathbf{TS_A}$ barrier. As a result, with ethylbenzene as a substrate the phenyl hydroxylation will take place on a dominant LS cationic surface (via $^2\mathbf{A_{cat}}$), while with benzene as a substrate competitive processes via $^2\mathbf{A_{cat}}$ and $^2\mathbf{A_{rad}}$ are possible. The HS pathway for phenyl hydroxylation encounters a high C–O bond-formation barrier followed by another high proton-shuttle barrier ($^4\mathbf{TS_C}$), whereas this process is barrierless on the LS pathway.

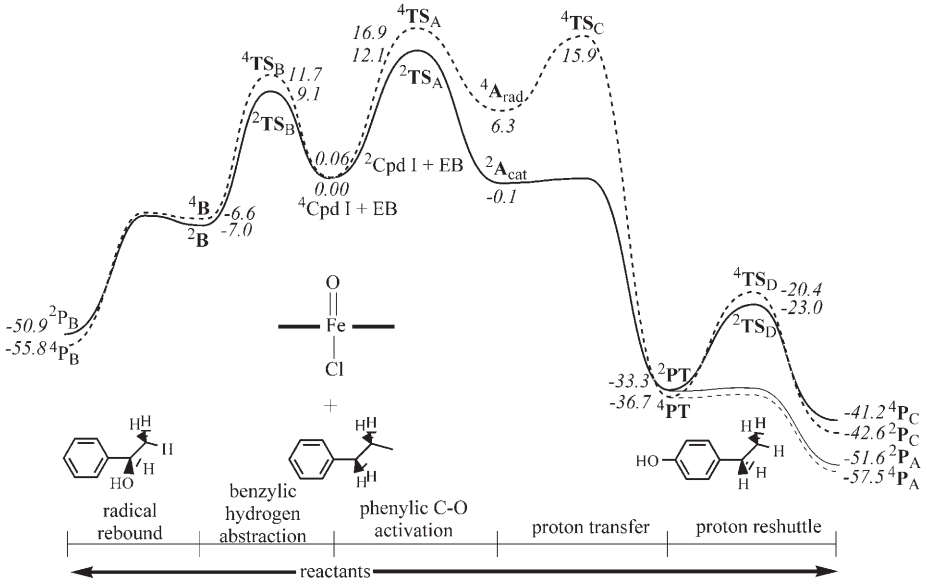

Figure 7. Energy profile with LACV3P+* energies and LACVP ZPE corrections for the reaction of ^{4,2}Cpd I with ethylbenzene (EB). The process starting in the centre and toward the left is the benzylic hydroxylation, whereas that to the right is the phenyl activation. All energies are in kcal mol^{-1} relative to the isolated reactants in the quartet spin state.

Thus, the energy difference in the gas phase between the lowest-lying benzyl and phenyl hydroxylation processes is 3.0 kcal mol^{-1}. To find out whether external or internal effects change the regioselectivity of the reaction, we show in Figure 8 the relative free-energy barriers of the reaction of [H_{10}]ethylbenzene and [D_{10}]ethylbenzene with ^{4,2}[(Fe=O)Cl(Por)] in different environments. In the gas phase and in apolar solvents, ^{4,2}[(Fe=O)Cl(Por)] reacts with [H_{10}]ethylbenzene mainly by benzyl hydroxylation via $^{4,2}\mathbf{TS_A}$, but an increase of the dielectric constant of the medium lowers the phenyl hydroxylation barrier via $^2\mathbf{TS_A}$ to within 0.5 kcal mol^{-1}. Although the dielectric constant does

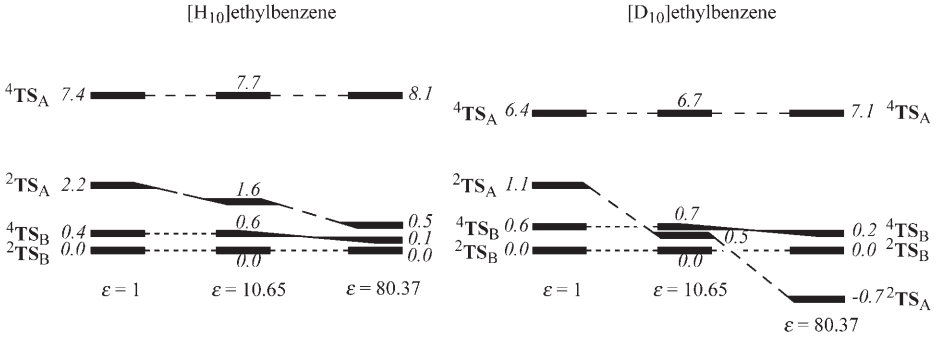

Figure 8. Relative free energies ($\Delta G^{\neq}$ in kcal mol^{-1} relative to $^2\mathbf{TS_B}$) of $^{4,2}\mathbf{TS_A}$ and $^{4,2}\mathbf{TS_B}$ in different environments using [H_{10}]ethylbenzene (left) and [D_{10}]ethylbenzene (right) as the substrate.

not change the relative ordering of the transition states in the reaction of ^{4,2}[(Fe=O)Cl(Por)] with [H_{10}]ethylbenzene, a significant amount of *p*-ethylphenol side products can be expected in a strongly polar solvent. However, replacing the hydrogen atoms by deuterium atoms in ethylbenzene destabilises the benzyl hydroxylation process (Table 2) as a benzylic C–D bond is stronger than a benzylic C–H bond. By contrast, the C–O formation barriers are hardly affected by isotopic substitution of hydrogen atoms. As a consequence, in the gas phase the energy separation between ^{2}**TS**$_{B}$ and ^{2}**TS**$_{A}$ is 2.2 kcal mol^{-1} for [H_{10}]ethylbenzene, whereas the gap is lowered to 1.1 kcal mol^{-1} for [D_{10}]ethylbenzene. A dielectric constant further stabilises ^{2}**TS**$_{A}$ with respect to ^{2}**TS**$_{B}$ because it represents a reaction barrier leading to a cationic intermediate, whereby the charge separation within the TS is stabilising. Indeed, as can be seen from Figure 8, the fully deuterated ethylbenzene will react to predominantly form *p*-ethylphenol in a polar solvent with a dielectric constant of 80.37, whereas [H_{10}]ethylbenzene will predominantly give benzyl hydroxylation products under all environmental conditions tested. Therefore, substitution of hydrogen by deuterium leads to a regioselectivity change in a polar solvent from dominant benzyl hydroxylation to phenyl hydroxylation. This regioselectivity change is accomplished due to 1) a larger C–D activation barrier than C–H activation barrier in ^{4,2}**TS**$_{B}$ and 2) the stabilising effect of a cationic process via ^{2}**TS**$_{A}$.

Conclusion

We have performed DFT calculations for the possible reaction mechanisms of ^{4,2}[(Fe=O)Cl(Por)] with ethylbenzene leading to 1-phenylethanol, *p*-ethylphenol and 4-ethylcyclohexa-2,4-dienone. The reactions occur via two-state reactivity patterns on competing low-spin and high-spin surfaces and the dominant pathway leads to 1-phenylethanol. However, our calculations show that replacing all of the hydrogen atoms in ethylbenzene by deuterium atoms destabilises the benzyl hydroxylation barriers so that the phenyl-activation mechanism becomes competitive. In particular, in an environment with a large dielectric constant, in which the charge-separated species in the phenyl-activation process are further stabilised, this process becomes the dominant factor. The results have been reported in the context of experimental work on oxo–iron–porphyrin catalysts as well as compared with studies on P450 enzymes.

Acknowledgements

The National Service of Computational Chemistry Software (NSCCS) is acknowledged for the CPU time it provided.

[1] M. Sono, M. P. Roach, E. D. Coulter, J. H. Dawson, *Chem. Rev.* **1996**, *96*, 2841–2887.
[2] W.-D. Woggon, *Top. Curr. Chem.* **1996**, *184*, 40–96.
[3] *The Porphyrin Handbook* (Eds.: K. M. Kadish, K. M. Smith, R. Guilard), Academic Press, San Diego, CA, **2000**.
[4] F. P. Guengerich, *Chem. Res. Toxicol.* **2001**, *14*, 611–650.
[5] J. T. Groves, *Proc. Natl. Acad. Sci. USA* **2003**, *100*, 3569–3574.
[6] B. Meunier, S. P. de Visser, S. Shaik, *Chem. Rev.* **2004**, *104*, 3947–3980.
[7] *Cytochrome P450: Structure, Mechanism and Biochemistry* (Ed.: P. R. Ortiz de Montellano), 3rd ed., Kluwer Academic/Plenum, New York, **2004**.
[8] M. H. Gelb, D. C. Heimbrook, P. Mälkönen, S. G. Sligar, *Biochemistry* **1982**, *21*, 370–377.
[9] a) I. Schlichting, J. Berendzen, K. Chu, A. M. Stock, S. A. Maves, D. E. Benson, R. M. Sweet, D. Ringe, G. A. Petsko, S. G. Sligar, *Science* **2000**, *287*, 1615–1622; b) R. Davydov, T. M. Makris, V. Kofman, D. E. Werst, S. G. Sligar, B. M. Hoffman, *J. Am. Chem. Soc.* **2001**, *123*, 1403–1415.
[10] S. Jin, T. A. Bryson, J. H. Dawson, *J. Biol. Inorg. Chem.* **2004**, *9*, 644–653.
[11] W. Nam, Y. O. Ryu, W. J. Song, *J. Biol. Inorg. Chem.* **2004**, *9*, 654–660.
[12] A. D. N. Vaz, D. F. McGinnity, M. J. Coon, *Proc. Natl. Acad. Sci. USA* **1998**, *95*, 3555–3560.
[13] a) F. Ogliaro, S. P. de Visser, S. Cohen, P. K. Sharma, S. Shaik, *J. Am. Chem. Soc.* **2002**, *124*, 2806–2817; b) P. K. Sharma, S. P. de Visser, S. Shaik, *J. Am. Chem. Soc.* **2003**, *125*, 8698–8699; c) D. Kumar, H. Hirao, S. P. de Visser, J. Zheng, D. Wang, W. Thiel, S. Shaik, *J. Phys. Chem. B* **2005**, *109*, 19946–19951.
[14] M. J. Park, J. Lee, Y. Suh, J. Kim, W. Nam, *J. Am. Chem. Soc.* **2006**, *128*, 2630–2634.
[15] W. M. Atkins, S. G. Sligar, *J. Am. Chem. Soc.* **1987**, *109*, 3754–3760.
[16] For examples of metabolic switching in P450 enzymes, see: a) C.-H. Yun, G. P. Miller, F. P. Guengerich, *Biochemistry* **2001**, *40*, 4521–4530; b) C. L. Shaffer, S. Harriman, Y. M. Koen, R. P. Hanzlik, *J. Am. Chem. Soc.* **2002**, *124*, 8268–8274.
[17] a) R. P. Hanzlik, K. Hogberg, C. M. Judson, *Biochemistry* **1984**, *23*, 3048–3055; b) R. P. Hanzlik, K. Hogberg, J. B. Moon, C. M. Judson, *J. Am. Chem. Soc.* **1985**, *107*, 7164–7167; c) R. P. Hanzlik, K.-H. J. Ling, *J. Org. Chem.* **1990**, *55*, 3992–3997.
[18] a) R. E. McMahon, H. R. Sullivan, J. C. Craig, W. E. Pereira, Jr., *Arch. Biochem. Biophys.* **1969**, *132*, 575–577; b) H. L. Holland, I. M. Carter, C. Chenchaiah, S. H. Khan, B. Munoz, R. W. Ninniss, D. Richards, *Tetrahedron Lett.* **1985**, *26*, 6409–6412; c) D. Filipovic, M. D. Paulsen, P. J. Loida, S. G. Sligar, R. L. Ornstein, *Biochem. Biophys. Res. Commun.* **1992**, *189*, 488–495.
[19] R. E. White, J. P. Miller, L. V. Favreau, A. Bhattacharyya, *J. Am. Chem. Soc.* **1986**, *108*, 6024–6031.
[20] a) J. T. Groves, P. Viski, *J. Am. Chem. Soc.* **1989**, *111*, 8537–8538; b) J. T. Groves, P. Viski, *J. Org. Chem.* **1990**, *55*, 3628–3634.
[21] W. J. Song, Y. O. Ryu, R. Song, W. Nam, *J. Biol. Inorg. Chem.* **2005**, *10*, 294–304.
[22] a) J. T. Groves, T. E. Nemo, *J. Am. Chem. Soc.* **1983**, *105*, 5786–5791; b) J. T. Groves, Z. Gross, M. K. Stern, *Inorg. Chem.* **1994**, *33*, 5065–5072; c) K. Czarnecki, S. Nimri, Z. Gross, L. M. Proniewicz, J. R. Kincaid, *J. Am. Chem. Soc.* **1996**, *118*, 2929–2935.
[23] For examples of the effects of the axial ligand on the reactivity of oxo–iron–porphyrins, see: a) Z. Gross, S. Nimri, *Inorg. Chem.* **1994**, *33*, 1731–1732; b) Z. Gross, *J. Biol. Inorg. Chem.* **1996**, *1*, 368–371; c) W. Nam, M. H. Lim, S.-Y. Oh, J. H. Lee, H. J. Lee, S. K. Woo, C. Kim, W. Shin, *Angew. Chem.* **2000**, *112*, 3792–3795; *Angew. Chem. Int. Ed.* **2000**, *39*, 3646–3649.
[24] a) S. P. de Visser, *J. Phys. Chem. A* **2005**, *109*, 11050–11057; b) S. P. de Visser, *Angew. Chem.* **2006**, *118*, 1822–1825; *Angew. Chem. Int. Ed.* **2006**, *45*, 1790–1793.
[25] S. P. de Visser, *J. Biol. Inorg. Chem.* **2006**, *11*, 168–178.
[26] S. Shaik, S. P. de Visser, F. Ogliaro, H. Schwarz, D. Schröder, *Curr. Opin. Chem. Biol.* **2002**, *6*, 556–567.
[27] a) A. D. Becke, *J. Chem. Phys.* **1993**, *98*, 5648–5652; b) C. Lee, W. Yang, R. G. Parr, *Phys. Rev. B* **1988**, *37*, 785–789.
[28] P. J. Hay, W. R. Wadt, *J. Chem. Phys.* **1985**, *82*, 299–310.

[29] Jaguar 5.5, Schrödinger, Inc., Portland, OR, **2000**.
[30] Gaussian 03, Revision C.01, M. J. Frisch, G. W. Trucks, H. B. Schlegel, G. E. Scuseria, M. A. Robb, J. R. Cheeseman, J. A. Montgomery, Jr., T. Vreven, K. N. Kudin, J. C. Burant, J. M. Millam, S. S. Iyengar, J. Tomasi, V. Barone, B. Mennucci, M. Cossi, G. Scalmani, N. Rega, G. A. Petersson, H. Nakatsuji, M. Hada, M. Ehara, K. Toyota, R. Fukuda, J. Hasegawa, M. Ishida, T. Nakajima, Y. Honda, O. Kitao, H. Nakai, M. Klene, X. Li, J. E. Knox, H. P. Hratchian, J. B. Cross, V. Bakken, C. Adamo, J. Jaramillo, R. Gomperts, R. E. Stratmann, O. Yazyev, A. J. Austin, R. Cammi, C. Pomelli, J. W. Ochterski, P. Y. Ayala, K. Morokuma, G. A. Voth, P. Salvador, J. J. Dannenberg, V. G. Zakrzewski, S. Dapprich, A. D. Daniels, M. C. Strain, O. Farkas, D. K. Malick, A. D. Rabuck, K. Raghavachari, J. B. Foresman, J. V. Ortiz, Q. Cui, A. G. Baboul, S. Clifford, J. Cioslowski, B. B. Stefanov, G. Liu, A. Liashenko, P. Piskorz, I. Komaromi, R. L. Martin, D. J. Fox, T. Keith, M. A. Al-Laham, C. Y. Peng, A. Nanayakkara, M. Challacombe, P. M. W. Gill, B. Johnson, W. Chen, M. W. Wong, C. Gonzalez, J. A. Pople, Gaussian, Inc., Wallingford CT, **2004**.
[31] a) S. P. de Visser, F. Ogliaro, P. K. Sharma, S. Shaik, *J. Am. Chem. Soc.* **2002**, *124*, 11809–11826; b) D. Kumar, S. P. de Visser, P. K. Sharma, S. Cohen, S. Shaik, *J. Am. Chem. Soc.* **2004**, *126*, 1907–1920.
[32] S. Shaik, D. Kumar, S. P. de Visser, A. Altun, W. Thiel, *Chem. Rev.* **2005**, *105*, 2279–2328.
[33] a) F. Ogliaro, S. P. de Visser, S. Cohen, J. Kaneti, S. Shaik, *ChemBioChem* **2001**, *2*, 848–851; b) S. P. de Visser, S. Shaik, P. K. Sharma, D. Kumar, W. Thiel, *J. Am. Chem. Soc.* **2003**, *125*, 15779–15788.
[34] S. P. de Visser, S. Shaik, *J. Am. Chem. Soc.* **2003**, *125*, 7413–7424.
[35] F. Ogliaro, N. Harris, S. Cohen, M. Filatov, S. P. de Visser, S. Shaik, *J. Am. Chem. Soc.* **2000**, *122*, 8977–8989.
[36] S. P. de Visser, D. Kumar, S. Cohen, R. Shacham, S. Shaik, *J. Am. Chem. Soc.* **2004**, *126*, 8362–8363.
[37] S. P. de Visser, F. Ogliaro, P. K. Sharma, S. Shaik, *Angew. Chem.* **2002**, *114*, 2027–2031; *Angew. Chem. Int. Ed.* **2002**, *41*, 1947–1951.

Received: March 16, 2006
Published online: July 26, 2006

